Energy Reports 9 (2023) 1637–1650

Contents lists available at ScienceDirect

Energy Reports

journal homepage: www.elsevier.com/locate/egyr

Research paper

Multi-objective optimization for simultaneously designing active control of tower vibrations and power control in wind turbines

Manuel Lara [a], Juan Garrido [a,*], Mario L. Ruz [b], Francisco Vázquez [a]

[a] Department of Electrical Engineering and Automation, University of Cordoba, Campus of Rabanales, 14071 Cordoba, Spain
[b] Department of Mechanics, University of Cordoba, Campus of Rabanales, 14071 Cordoba, Spain

ARTICLE INFO

Article history:
Received 19 September 2022
Received in revised form 20 December 2022
Accepted 27 December 2022
Available online 4 January 2023

Keywords:
Wind turbine
Multi-objective optimization
Vibration mitigation
Active tower damping control

ABSTRACT

For wind turbines operating in the full load region, stabilizing the generated power at its nominal value is a key objective. Furthermore, the control of tower vibrations is a major constraint in wind turbine structures because diverse loading sources can induce fatigue damage. These goals are often conflicting, and a trade-off solution must be found. To reduce tower vibrations, an additional damping method can be implemented by ensuring coordination between the pitch and torque control scheme. This study proposes a control scheme that balances these two objectives: power generation and tower vibration reduction. The control design is based on a collective pitch combined with two active tower damping controls: one for frontal oscillations to the wind, which generates an extra pitch component, and another for lateral displacements, which produces an additional component of the generator torque. The control parameters are tuned through multi-objective optimization and multi-criteria decision methods with FAST software along with MATLAB/Simulink. The proposed control scheme was simulated according to the extreme wind direction change in the IEC 61400–1 standard. The results show that the proposed procedure achieves a notable reduction in tower vibrations, whereas the generated power is almost unaffected. To support this conclusion, a set of performance indices and the time and frequency responses are analyzed from the simulations Comparisons with other control schemes illustrate the superior performance of the proposed methodology.

1. Introduction

Faced with the challenge of global warming, renewable energies have experienced great growth to reduce greenhouse gas emissions, cope with the increase in energy demand, and avoid high dependence on energy imports. In this massive deployment of renewables, wind energy has played a key role in recent decades. The total worldwide wind capacity in 2021 reached 837 GW, with China, USA, Germany, India, and Spain together accounting for 72%. Even so, according to the forecast of the International Energy Agency, wind power capacity must increase up to 3200 GW by 2030 to limit global warming to 1.5 °C (Lee and Zhao, 2022). For this expansion to be financially affordable and competitive, wind power technology must keep improving its efficiency in energy production and reducing its maintenance costs as well (Luo et al., 2019). From a control viewpoint, these costs can be significantly reduced by operating wind turbines more efficiently: improving the power captured from the wind and, simultaneously, reducing their different structural loads to increase their fatigue life (Kong et al., 2017).

Nowadays, three-bladed variable speed and variable pitch (VSVP) wind turbines are the most widespread because their control system allows them to work in different operational regions according to the wind speed (Gambier, 2021). Between the cut-in wind speed and the rated wind speed (partial load region), the control system aims to capture as much power as possible from the wind by tracking the optimal generator characteristic (Saravanakumar and Jena, 2015; Yin et al., 2018). In this region, the generator torque control allows the wind turbine speed to vary while the collective pitch angle remains at its minimum value (Song et al., 2022; Yin et al., 2017). The full load region is defined over the rated wind speed and below the cut-off value. In this region, the objective is to regulate the generator power at its rated value over various wind speeds. For this aim, the control system pitches the blades to enable smooth power production and reduce mechanical loads and vibrations (Novaes Menezes et al., 2018). A transition region, which is defined around the rated wind speed value when the torque is still below its rated value, is generally used to ensure a smooth switch between the respective controllers of the partial load region and the full load region (Ruz et al., 2020; Fragoso et al., 2017).

* Corresponding author.
E-mail addresses: p12laorm@uco.es (M. Lara), juan.garrido@uco.es (J. Garrido), mario.ruz@uco.es (M.L. Ruz), fvazquez@uco.es (F. Vázquez).

https://doi.org/10.1016/j.egyr.2022.12.141

Nomenclature

Acronyms

AGTC	Active generator-torque control
ATDC	Active tower damping control
CPC	Collective pitch control
CVR	Cumulative variation rate
EDC	Extreme direction change
FA	Fore–aft
FFT	Fast Fourier transform
GA	Genetic algorithm
IPC	Individual pitch control
ISE	Integral of the square error
MCDM	Multi-criteria decision-making
MOO	Multi-objective optimization
NSGA	Non-dominated sorting genetic algorithm
PID	Proportional–integral–derivative
SAW	Simple additive weighting
SS	Side–side
STD	Standard deviation
TFC	Tower feedback control
TOPSIS	Technique for order of preference by similarity to ideal solution
VIKOR	VlseKriterijumska optimizacija I kompromisno resenje
VS-VP	Variable speed, variable pitch

Symbols

CVR_D	CVR of total tower displacement
D	Tower model damping
F	Rotor thrust
h	Sampling period
I(k)	Integral action in the kth sampling period
J	Cost function
K	Tower model stiffness
K_{FA}	Gain of TFC
K_P	Proportional gain
K_{SS}	Gain of AGTC
M	Tower model mass
P_g	Generated power
P(k)	Proportional action in the kth sampling period
STD_{x+y}	Sum of the displacement STDs in FA and SS directions
T_g	Generator torque
T_I	Integral time constant
x or x_{FA}	Nacelle fore–aft displacement
$x_{FA,0}$	Tower-top fore–aft displacement in the tower frame
$x_{FA,\theta}$	Tower-top fore–aft displacement in the nacelle frame rotated a yaw angle θ
y or y_{SS}	Nacelle side–side displacement
$y_{SS,0}$	Tower-top side–side displacement in the tower frame
$y_{SS,\theta}$	Tower-top side–side displacement in the nacelle frame rotated a yaw angle θ
β	Pitch angle
β_{CPC}	Pitch angle provided by the CPC
β_{FA}	Pitch angle provided by the TFC
θ	Nacelle yaw angle with respect to the initial tower reference frame
θ_v	Wind direction
v	Mean wind speed
$\tau_{g,SS}$	Generator torque provided by the AGTC
ω_g	Rotational generator speed
δ	Change, difference
∂F	Extra thrust force

Wind turbine control in the full load region is challenging due to the complex and non-linear dynamics of the system, the coupling of its variables, and the uncertainty of wind conditions. When wind speed is over the rated value, the power must be limited by the corresponding controller, which in the case of VS-VP wind turbines produces a collective pitch control (CPC) signal β_{CPC} to pitch all blades simultaneously at the same angle. The generator torque T_g (N m) is usually fixed at its rated value T_{g_rated} and therefore, according to (1), the power output P_g (W) can indirectly be maintained constant at its rated value using a control loop of the rotational speed ω_g (rad/s).

$$P_g = T_{g\_rated} \cdot \omega_g \tag{1}$$

The most classical approach applied to the CPC is the Proportional–Integral–Derivative (PID) control (Novaes Menezes et al., 2018), which is usually implemented with gain scheduling to adapt to the wind turbine dynamic changes with the wind speed (Bianchi et al., 2007; Jonkman et al., 2009). To enhance the performance of classical PID controllers, some authors propose using more modern versions of PID control, such as nonlinear PID controllers, which adjust the control parameters from nonlinear functions of the error signal, or fractional PID controllers, which add new tuning parameters (Gambier, 2022a). More advanced control methods have also been studied. In Yuan and Tang (2017), a disturbance accommodation controller with model reference adaptive control is developed for pitch control to regulate the generator speed and to reduce induced load in a wind turbine with structural uncertainties. In Wakui et al. (2021), model predictive control (MPC) is applied to wind turbines with a formulation that considers additional objectives and constraints, such as pitch usage, power limit, or tower displacements; however, it uses wind turbine models linearized around some operation point, and consequently, the model uncertainties can lead to errors in the analysis. To address this issue, some authors used nonlinear MPC (Schlipf et al., 2013) or applied robust control to nonlinear wind turbine models (Faraji Nayeh et al., 2020; Garcia-Sanz and Houpis, 2012). Recently, intelligent control approaches, such as fuzzy control (Viveiros et al., 2015), neural networks (NNs), or reinforcement learning (RL), have been developed for CPC of wind turbines to improve their performance (Sierra-García and Santos, 2021). These methods can be used to directly design the pitch controller or can be combined with other controllers in hybrid strategies. In Sierra-García and Santos (2020), an NN is trained and implemented as a pitch controller to maintain the power output at the rated value. In Sierra-Garcia and Santos (2022), the pitch control combines a fuzzy logic controller and a deep learning module that also estimates the effective wind. In Sierra-Garcia et al. (2022), the same authors propose a hybrid control that combines an RL-based controller with a PID regulator for CPC, and they achieve speeding up the learning

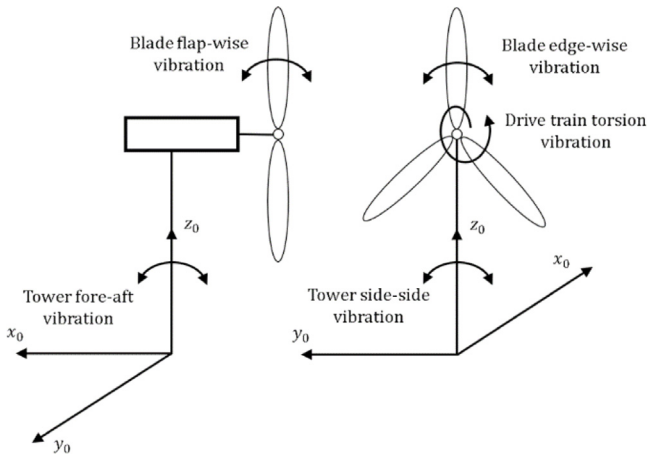

Fig. 1. Different wind turbine oscillations and initial tower reference frame.

convergence and reduce the error of the power output compared with a PID controller.

In addition to the power output regulation, in the full load region, mitigation of structural loads and oscillations is crucial to avoid undesirable effects or even early failure of the wind turbine. These loads can produce different vibration modes with strong coupling among them, as shown in Fig. 1. The tower fore–aft oscillations show strong coupling with the blade flap-wise vibration, while the tower side–side fluctuations and the blade edge-wise vibrations are strongly coupled with the drive torsional vibration (Liu et al., 2016). The oscillation modes of the tower have been studied in a wide variety of works from different approaches: passive and active methods (Zuo et al., 2020). Passive or semi-active tuned mass dampers, calibrated liquid column dampers, or 3D pendulums installed in the nacelle can reduce the undesired tower oscillations (Fitzgerald et al., 2013; Galán-Lavado and Santos, 2021; Mensah and Dueñas-Osorio, 2014; Sun, 2018; Villoslada et al., 2021). Nevertheless, these additional devices incur extra installation and maintenance costs. In contrast, active tower damping control (ATDC) uses feedback to inject damping into the system through extra pitch or torque controllers. Cyclic loads due to the periodic rotation of the rotor occur at different frequencies and affect mainly the rotor blades. They can be reduced by individual pitch control (IPC), which individually adjusts the pitch of each blade (Bossanyi, 2003a). Feedforward control is another strategy that can be used to mitigate load and improve the generated power. This strategy uses wind speed measurements, typically provided by light detection and ranging (LIDAR) based technology, to generate a feedforward control signal that reduces fatigue in different parts of the wind turbine (Mahdizadeh et al., 2021; Schlipf et al., 2013; Wang et al., 2013). This feedforward signal is usually a pitch component that is combined with the CPC.

The tower oscillations in the fore–aft (FA) direction can be actively reduced by a complementary tower-feedback controller (TFC) that adds an extra pitch value β_{FA} (°) to the collective pitch signal β_{CPC} (°) (Fischer et al., 2012; Gambier and Nazaruddin, 2018). Tower dynamics in the fore–aft direction can be modeled according to (2), as a second-order system with a damped harmonic motion, where x_{FA} (m) is the fore–aft tower displacement, F (N) is the rotor thrust force, and M, D, and K are the tower modal mass, damping, and stiffness, respectively, in N/m. The term ∂F is the extra thrust force produced by the pitch increment $\Delta\beta$ (or β_{FA}) of the TFC. If this term ∂F is forced by $\Delta\beta$ to be proportional to $-\dot{x}_{FA}$ (m/s), as shown in (3), then, the effective damping of (2) can be increased an additional quantity D_{FA} (N s/m) (Bossanyi, 2003b). The tower-top fore–aft acceleration can be measured and integrated to provide an estimate of $\dot{x}_{FA}$. According to (4), the TFC signal β_{FA} can be obtained from a simple proportional control law with gain K_{FA} (N s/m), which is a design parameter to be tuned (Bossanyi, 2003b). Due to the nonlinear dynamics of wind turbines, some works propose that the gain K_{FA} be adaptive (Pascu et al., 2017).

$$M\ddot{x}_{FA} + D\dot{x}_{FA} + Kx_{FA} = F + \partial F \tag{2}$$

$$\partial F = \left(\frac{\partial F}{\partial \beta}\right)\Delta\beta = -D_{FA}\dot{x}_{FA} \tag{3}$$

$$\beta_{FA} = \Delta\beta = \frac{-D_{FA}}{(\partial F/\partial\beta)}\dot{x}_{FA} = K_{FA}\dot{x}_{FA} \tag{4}$$

The control actions of CPC and TFC are coupled since both actions converge to the same control variable, the pitch angle. They are also contradictory. When the CPC produces strong pitch variations to limit the power output, which is even more frequent in the presence of wind turbulence, the tower vibrations increase. Subsequently, TFC modifies the pitch angle acting against the CPC to reduce the oscillations. This trade-off between power performance and fluctuation reduction in wind turbine control is addressed by some authors as a multi-objective optimization (MOO) problem. This approach is based on obtaining solutions from the Pareto front and the use of decision-makers. The Pareto solutions are optimal in the sense that no objective function can be improved without worsening others. Genetic algorithm (GA) methods can be used to identify correct and accurate Pareto fronts independently of the objectives and constraint functions, at the expense of many iterations and computational efforts (Chiandussi et al., 2012). Then, front solutions are analyzed and ranked through multi-criteria decision-making (MCDM) methods to select one of them according to the specific preferences (Gambier, 2022b; Lee and Chang, 2018). Recent works use MOO techniques to tune a more efficient control of wind turbines in simulated models. In Odgaard et al. (2016), a linear MPC is tuned considering Pareto optimality for power and fore–aft fatigue control of a wind turbine. In Gambier and Behera (2018), MOO is used to design CPC for power performance, TFC for tower oscillations, and IPC for loads on the blades. The work by Lara et al. (2021) proposes a gain scheduling PI controller for CPC, an adaptive gain for TFC, and an adaptive feedforward compensation for the wind speed. The controllers are tuned on the basis of a Pareto optimization problem that minimizes the generator speed error and the tower fore–aft displacements. The proposed solution achieves better performance than that obtained by a classical baseline PI controller. Most of these studies related to optimization and control methodologies for wind turbines use FAST (Fatigue, Aerodynamics, Structures, and Turbulence) software (Jonkman and Buhl, 2005) to validate their designs in simulation. This software allows representing the aeroelastic and dynamic characteristics of a wind turbine without physically depending on the natural resources of the wind and a real system. Works testing designs directly in real wind turbines are unusual.

Additionally, tower oscillations in the side–side (SS) direction can arise in wind turbines due to changes in the mean wind direction or wave loads in the case of offshore turbines. In Park et al. (2020), orthogonal tuned liquid column damper designs are optimized via multi-objective optimization to reduce fore–aft and side–side fatigue, and extreme loads. Other studies propose to compensate for lateral tower vibrations using active generator-torque control (AGTC), which can provide damping to these oscillations, as was demonstrated by Zhang et al. (2014). The generator torque affects the side–side tower vibrations through the reaction on the generator stator, which

is rigidly fixed to the nacelle. AGTC involves an ATDC method similar to that of TFC. Here, the control action $\tau_{g,SS}$ is added for damping to the demanded nominal value $\tau_{g,rated}$ in the full load region. These extra torque signals are calculated via feedback from the tower side–side velocity, $\dot{y}_{ss}$ (m/s), as shown in (5), and they are usually limited within ±10% of the rated generator torque. The tuning parameter is the gain K_{SS} (N s) and the lateral velocity can be obtained from measuring and integrating the tower-top side–side acceleration.

$$\tau_g = \tau_{g,rated} + \Delta\tau_g = \tau_{g,rated} + K_{SS}\dot{y}_{SS} \tag{5}$$

The reduction of lateral tower vibrations is also related to the mitigation of edgewise deflection modes of the blades. The generator torque is used as a way to dampen the torsional vibrations of the drivetrain (Poureh and Nobakhti, 2020). However, the tower AGTC can increase the fluctuations in the power output. In Golnary and Tse (2022), this trade-off between reducing power output fluctuations and tower lateral oscillations is addressed by simultaneously using a fuzzy torque control and a sliding mode pitch controller. Nevertheless, this study does not consider the tower fore–aft oscillations in its proposed control scheme. Recently, some authors have proposed coordinated pitch and torque methodologies based on MPC and Pareto optimization to reduce mechanical loads and improve power output (Lin et al., 2018, 2019; Song et al., 2022).

There are few studies dealing simultaneously with AGTC of tower vibrations and power control regulation (Golnary and Tse, 2022). To the best of our knowledge, works dealing simultaneously with minimizing power fluctuations, tower fore–aft vibration, and tower side–side oscillations in the full load region are even more unusual in the literature. Additionally, there is a trade-off between these three objectives that needs to be considered. To address this research gap, we combine CPC, TFC, and AGTC in a control scheme with three loops, and we tune the controllers using a multi-objective optimization on a 5 MW wind turbine that is simulated with FAST software and MATLAB/Simulink. The optimization considers one objective function of the generated power error and two indices associated with the tower vibrations. Other simpler control strategies considering fewer control loops are also developed and optimized for performance comparison. The results demonstrate that simultaneously adding active damping through both pitch loop and generator-torque loop to a conventional collective pitch controller considerably reduces the tower vibrations of the wind turbine without significatively affecting the generated power.

The rest of the paper is organized as follows: Section 2 introduces the full proposed control scheme for the wind turbine in the full load region and defines the parameters to be tuned. In Section 3, the objectives to minimize are described and the MOO problem is formulated. An illustrative example and the simulation results are exposed in Section 4, and finally, conclusions are discussed in Section 5.

2. Control system

The scheme of the proposed wind turbine control system in the full load region is shown in Fig. 2. The controlled variables are the generator speed ω_g, the nacelle fore–aft and side–side displacements x_{FA} and y_{SS}, and the nacelle yaw angle θ with respect to the initial tower reference frame. The measurements required by the control system are generator speed, fore–aft and side–side top-tower accelerations, pitch angles, nacelle yaw angle, generator power, and wind speed and direction. All these variables are assumed to be obtained from conventional sensors installed in the wind turbine.

A CPC implemented with a PI controller regulates the generator speed at its nominal value, $\omega_{g,rated}$. The controller produces the control signal β_{CPC} to reject the wind speed disturbances according to (6). Its tuning parameters are the proportional gain K_P (°/rpm) and the integral time constant T_I (s).

$$\beta_{CPC} = K_P\left(\omega_{g,rated} - \omega_g(t)\right) + \frac{1}{T_I}\int\left(\omega_{g,rated} - \omega_g(t)\right)dt \tag{6}$$

The tower fore–aft oscillations are compensated by a TFC, which adds an extra pitch signal β_{FA} to the pitch value generated by the CPC. This β_{FA} signal is calculated according to (4) and is proportional to the fore–aft nacelle velocity.

The control laws are discretized according to the Tustin approximation with a sampling period of h seconds and implemented with the difference equations in (7). The proportional term P(k) and integral term I(k) in the kth iteration are defined in (7)(a) and (7)(b). Eq. (7)(c) defines the TFC action, which provides the pitch component β_{FA}. The initial pitch signal β(k) is the sum of proportional and integral components plus the TFC term, as shown in (7)(d). The first "if" clause (7)(e) limits the pitch signal considering its slew rate constraint $|\Delta\beta_{max}|$. The second "if" clause (7)(f) is an anti-windup mechanism that copes with the pitch limits β_{min} and β_{max} and updates the integral term I(k) within its limits when the pitch value is out of range.

$$\begin{aligned}
&(a)\ P(k) = K_P\left(\omega_{g,rated} - \omega_g(k)\right)\\
&(b)\ I(k) = I(k-1) + \frac{K_P h}{2T_I}\left(\omega_{g,rated} - \omega_g(k)\right.\\
&\quad\left. + \left(\omega_{g,rated} - \omega_g(k-1)\right)\right)\\
&(c)\ \beta_{FA}(k) = K_{FA}\dot{x}_{FA,\theta}(k)\\
&(d)\ \beta(k) = P(k) + I(k) + \beta_{FA}(k)\\
&(e)\ \textit{if}\ \beta(k) - \beta(k-1) < -h\cdot|\Delta\beta_{max}|\\
&\qquad \beta(k) = \beta(k) - h\cdot|\Delta\beta_{max}|\\
&\quad \textit{elseif}\ \beta(k) - \beta(k-1) > h\cdot|\Delta\beta_{max}|\\
&\qquad \beta(k) = \beta(k) + h\cdot|\Delta\beta_{max}|\\
&\quad \textit{end}\\
&(f)\ \textit{if}\ \beta(k) < \beta_{min}\\
&\qquad I(k) = \beta_{min} - P(k) - \beta_{FA}(k)\\
&\quad \textit{elseif}\ \beta(k) > \beta_{max}\\
&\qquad I(k) = \beta_{max} - P(k) - \beta_{FA}(k)\\
&\quad \textit{else}\\
&\qquad I(k) = \beta(k) - P(k) - \beta_{FA}(k)\\
&\quad \textit{end}
\end{aligned} \tag{7}$$

The tower lateral vibrations are damped by the AGTC, which produces an extra component $\tau_{g,SS}$ of the generator torque to be added to the rated torque. This extra component is proportional to the nacelle side–side velocity, as shown in (5). The final torque signal is constrained considering the slew rate and saturation limits of the generator. In most works, the extra component $\tau_{g,SS}$ is constrained to ±10% of the rated generator torque (Golnary and Tse, 2022).

The control signals produced by the TFC and AGTC are proportional to the nacelle velocities in the fore–aft and side–side directions, respectively. In this work, we assume that the accelerations of the tower top are measured by sensors mounted perpendicularly at the tower top, as provided by the FAST software in simulations, and then, they are integrated to obtain the tower top velocities. Therefore, these velocities are obtained in the initial tower reference frame with x_0- and y_0-axes, as shown in Fig. 1. When the nacelle orientation matches the initial tower frame, as depicted in Fig. 1, tower-top velocities directly provide

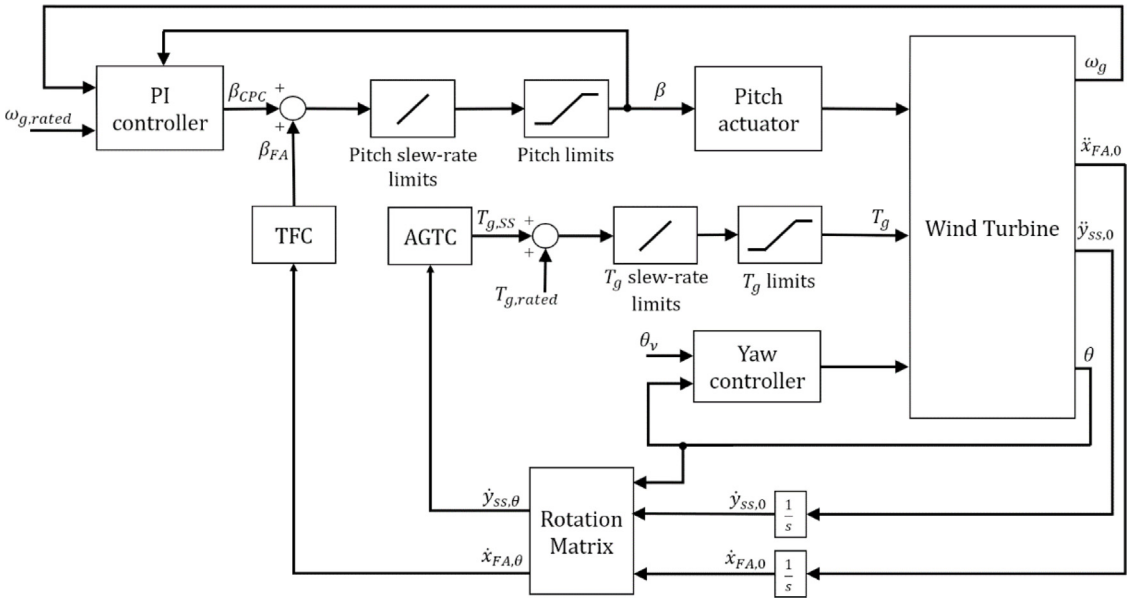

Fig. 2. Proposed control system scheme.

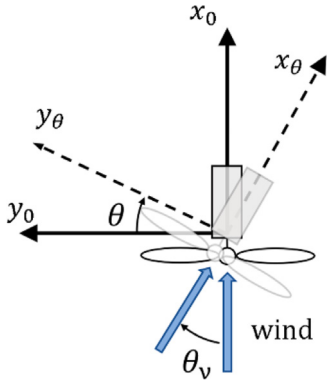

Fig. 3. Rotation transformation from the tower reference frame to the nacelle reference frame.

the required nacelle velocities. However, when the mean wind direction changes, the yaw controller begins to rotate the nacelle until reducing the mean yaw misalignment with the mean wind direction. In the desired stationary situation, the wind is frontal to the nacelle fore–aft direction and perpendicular to the nacelle side–side direction. If the nacelle and its moving reference frame, with x_θ- and y_θ-axes, have rotated a yaw angle θ (°) with respect to the initial tower frame, as depicted in Fig. 3, the tower-top velocities do not fit the nacelle velocities required by the TFC and AGTC for damping. Therefore, the tower top velocities must be transformed from the initial tower frame to the nacelle frame using the rotation matrix in (8), where $\dot{x}_{FA,0}$ and $\dot{y}_{SS,0}$ are the measured fore–aft and side–side tower-top velocities in the tower frame, respectively. And $\dot{x}_{FA,\theta}$ and $\dot{y}_{SS,\theta}$ are the corresponding velocities in the nacelle frame rotated a yaw angle θ with respect to the initial tower frame.

$$\begin{pmatrix} \dot{x}_{FA,\theta} \\ \dot{y}_{SS,\theta} \end{pmatrix} = \begin{pmatrix} \cos(\theta) & \sin(\theta) \\ -\sin(\theta) & \cos(\theta) \end{pmatrix} \begin{pmatrix} \dot{x}_{FA,0} \\ \dot{y}_{SS,0} \end{pmatrix} \tag{8}$$

The yaw controller used in this work is the pre-defined control referred to as the baseline in Spencer et al. (2012). It works in an on–off manner to avoid the yaw action to be enabled continuously. This controller rotates the nacelle yaw angle to follow the mean wind direction θ_v determining the yaw rate according to the following procedure: first, if the error between the current yaw angle and the 30-s time-averaged wind direction is greater than 5°, the controller begins yawing at 0.3°/s. Then, it stops yawing when the error between the current yaw angle and the 2-s time-averaged wind direction is less than 0.5°. The time-averaged wind direction is computed for each sampling time of 0.02 s using a discrete function. The operation of the yaw controller is independent of the other control blocks: CPC, TFC, and AGTC, whose tuning procedure is explained in the next section.

3. Tuning procedure by multi-objective optimization

3.1. MOO formulation

The control scheme described in the previous section has three control blocks to be tuned: CPC, TFC, and AGTC. Four parameters require tuning: K_P and T_I for the PI controller of CPC, K_{FA} gain for TFC, and K_{SS} gain for AGTC. Each control block is intended to reach different conflictive objectives. Therefore, the tuning procedure of these controllers can be solved through MOO to achieve a proper trade-off between the design objectives. The decision variables match the previous tuning parameters and define the parameter vector $\rho = [K_P\ T_I\ K_{FA}\ K_{SS}]$. Three objective functions are proposed in the cost function vector J as follows:

$$J = [ISE_{Pg}\ STD_{x+y}\ CVR_D]^T. \tag{9}$$

The first one is the integral of the squared error between the rated power $P_{g,rated}$ and the generated power P_g, as shown in (10). This performance index is related to the generator speed regulation by the CPC. The ISE_{Pg} is used to penalize the control designs that produce large variations of the generated power with respect to its rated value.

$$ISE_{Pg} = \int \left(P_{g,rated} - P_g(t)\right)^2 dt \qquad (W^2s) \tag{10}$$

The other two cost functions to be reduced are associated with mitigating the tower structural fatigue. The index STD_{x+y} (m) is the sum of the standard deviations of the tower vibration in the x_0- and y_0-axes, as shown in (11). Reducing STD_{x+y} involves decreasing the tower vibration amplitudes in these axes. The STD

has been previously used as a cost function to reduce the fatigue loads of the tower because they are correlated (Lackner and Rotea, 2011; Park et al., 2020; Villoslada et al., 2022). In addition, the STD reduction of the tower displacements is positively correlated to the STD reduction of tower moments (He et al., 2017). The STD considers the tower displacement amplitude but not its frequency, which is also related to the tower damage. To this purpose, this work proposes the cumulative variation rate of the tower displacements CVR_D. The index CVR_D (m) is defined in (12). Reducing CVR_D implies lowering the tower oscillation frequency. It considers the total tower displacement as the combination of two perpendicular components of movement: fore–aft and side–side . Both indices are simultaneously related to the TFC and AGTC, and they conflict with the ISE_{Pg} index. These three cost indices are computed from the time series data after completing a simulation; integrals and derivatives are replaced by discrete numerical approximations.

$$STD_{x+y} = STD_{FA} + STD_{SS} \tag{11}$$

$$CVR_D = \int \left(\sqrt{\left(\frac{dx_{FA}}{dt}\right)^2 + \left(\frac{dy_{SS}}{dt}\right)^2} \right) dt = \int \left(\sqrt{\dot{x}_{FA,0}^2 + \dot{y}_{SS,0}^2} \right) dt \tag{12}$$

The proposed MOO is performed according to the procedure depicted in Fig. 4. Once the conflicting cost functions are defined and the parameter vector is randomly initialized, the optimizer must obtain the Pareto front, which is a set of optimal solutions. A Pareto front solution is a non-dominated solution in the sense that no objective can be improved without degrading the others (Cui et al., 2017; Odgaard et al., 2016). The proposed objective functions cannot be evaluated analytically because they and the dynamic model of the wind turbine are very complex. Thus, a simulation-based approach is applied to obtain the Pareto front solutions by the optimizer. FAST software in conjunction with MATLAB/Simulink is used to simulate the proposed control system in Fig. 2. This nonlinear optimization requires an intensive computational effort and time; therefore, the optimizer uses the non-dominated sorting genetic algorithm-II (NSGA-II), which is an evolutionary algorithm specially developed for MOO (Deb et al., 2002), to achieve better computational efficiency. The main parameters configured in the genetic algorithm are as follows: a maximum generation of 100, a population size of 200, a Pareto front population fraction of 0.25%, and a crossover fraction of 0.8. The search range for K_P, T_I and K_{FA} is limited from 10^{-4} to 50, while K_{SS} ranges from 0 to $5 \cdot 10^5$. This range is determined prior to optimization by manually performing a bisection-like method in which the range is narrowed by discarding parameters that imply instability or too slow responses in the simulation.

Pareto fronts were calculated with a size of 50 points. One of these points must be selected to obtain the optimal controller parameters. Since there is a trade-off between the different objectives, MCDM methods are necessary to evaluate the optimal solutions and choose one according to specific preferences. Three common MCDM methods are SAW, TOPSIS, and VIKOR (Wang et al., 2016). Simple Additive Weighting (SAW) is considered to be the most intuitive and simple method. In SAW, the overall score of a candidate solution is calculated from the weighted sum of all attribute values. TOPSIS method defines two points: the positive ideal solution, which minimizes the cost criteria, and the negative ideal solution, which maximizes the cost criteria. Then, TOPSIS selects the solution with the shortest Euclidean distance from the positive ideal solution and the farthest Euclidean distance from the negative ideal solution (Wang et al., 2016). In the VIKOR method, the closest solution to the ideal one is preferred. The alternatives are evaluated according to the different criteria and ranked by comparing the closeness measure to the ideal solution (Chitsaz and Banihabib, 2015). In this work, the three previous MCDM methods are applied to each point of the calculated Pareto front and the average of them for each point is determined. Then, the solutions are ranked and the best one is selected as the best satisfactory solution. The tuning parameters associated with this solution are considered the optimal ones.

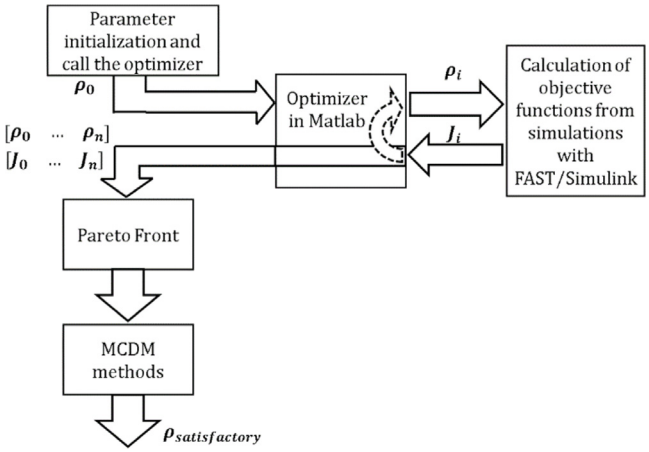

Fig. 4. Optimization process.

Table 1
Properties of the NREL 5-MW wind turbine.

Property	Value
Rated power	5 MW
Cut-In, Rated rotor speed	6.9 rpm, 12.1 rpm
Cut-In, Rated, Cut-out wind speed	3 m/s, 11.4 m/s, 25 m/s
Drivetrain	High-speed, multiple-stage gearbox
Rated generator speed	1173.7 rpm
Rated generator torque	43 093.55 N m
Gearbox ratio	97 :1
Electrical generator efficiency	94.4%
Rotor, Hub diameter	126 m, 3 m
Hub height	90 m
Rotor mass	110 000 kg
Nacelle mass	240 000 kg
Tower mass	347 460 kg
Limits on the blade pitch angle	0°–90°
Slew-rate limits on the pitch actuator	8°/s
Slew-rate limits on the generator torque	15 000 N m/s

4. Illustrative example

In this section, the proposed methodology is applied to the NREL 5-MW baseline wind turbine as an illustrative example. This turbine is based on the Repower 5 MW commercial model, a three-bladed VS-VP turbine. Its model is implemented by the software FAST version 8 and its main properties are collected in Table 1; more information about this turbine can be found in Jonkman et al. (2009). In this work, it is used as an onshore wind turbine.

The proposed Full Control has all three blocks enabled, i.e., CPC+TFC+AGTC. Additionally, the following combinations have also been designed and simulated for comparison: the CPC+TFC excludes the AGTC; the CPC+AGTC disables the TFC; and the CPC, which is the simplest one, only has the PI controller without TFC nor AGTC. These four control systems are implemented in Simulink with a sample period of 0.02 s.

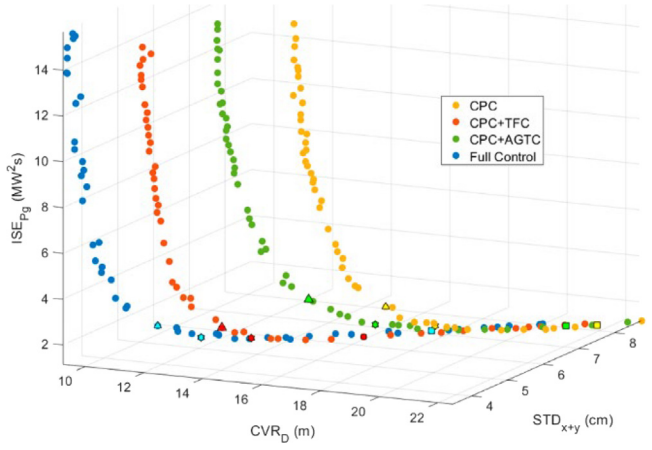

Fig. 5. 3D Pareto front points obtained for the EDC test.

4.1. Pareto fronts

For each control system, the described MOO procedure is performed to obtain the 3D Pareto fronts by considering the three objectives proposed in Section 3. The simulation performed throughout the optimization process consists of an extreme change in the wind direction defined according to the Extreme Direction Change (EDC) event of the IEC 61400–1 standard (IEC 61400–1, 2005). Simulations are performed with a total time of 700 s; however, the first 200 s are discarded to exclude transient effects in the data. The sampling frequency is set to 50 Hz. The required turbulent wind field is generated using TurbSim (Jonkman, 2009). Configured parameters are a turbulence intensity of approximately 14% and a power-law vertical shear with exponent 0.2 according to the Kaimal turbulence model defined by the Normal Turbulence Model Class B in the standard. The mean wind speed is 15 m/s and the wind direction changes about −30° in the horizontal plane in 200 s (within the 500 s selected from the simulation time). This event is intended to study the possible performance improvements that can be obtained under extreme conditions.

The resultant Pareto front points of each control system are shown in Fig. 5. Fig. 6 shows the 2D projections of these 3D Pareto fronts for ease of analysis. The combined use of TFC and AGTC in the Full Control improves the indices because the achieved Pareto front solutions have minor index values than those obtained using the other control systems. In the first and second plots of Fig. 6, the Pareto front of Full Control shifts further to the left than the other fronts, which means that minor CVR_D and STD_{x+y} values are obtained using the Full Control while the ISE_{Pg} value remains the same. After Full Control, the CPC+TFC achieves the best indices, whereas the CPC obtains the worst ones. The third plot of Fig. 6 indicates a correlation between the CVR_D and STD_{x+y} indices, which implies that minimizing one of them also reduces the other.

The final step for optimizing each control system is the selection of the best Pareto front point by considering the trade-off between objectives according to the different MCDM methods: SAW, TOPSIS, and VIKOR. Then, the averaged ranking solution is calculated for each control system. In this example, the TOPSIS solution and the averaged ranking solution are the same for each control approach. SAW, VIKOR, and proposed satisfactory ranked solutions are highlighted for each control system as squares, triangles, and stars, respectively, in Fig. 5. The averaged ranking solutions are also emphasized in Fig. 6. The optimal control parameters are those associated with these ranking solutions and are summarized in Table 2. Related objective indices are also shown.

Fig. 7 shows the spider diagram of the three optimized objective indices normalized with respect to those achieved by the CPC. The Full Control achieves the best indices related to the tower displacements, showing a reduction of 31.08% in the CVR_D with respect to that of the CPC, and a reduction of 24.19% in the STD_{x+y}. The ISE_{Pg} is slightly increased by 3.74%. The CPC+TFC achieves similar results to the Full Control and even a minor increase of 2% in the ISE_{Pg}. However, the reductions for the indices related to the tower displacements are less than 25%, not as low as those achieved with Full Control. The CPC+AGTC obtains a small increase of 4.14% in the ISE_{Pg} without reductions in the tower vibration indices as significant as in the previous two controls.

4.2. Simulation results

This section shows and analyzes the simulation results of the four control systems tuned with the previous optimal parameters in Table 2. The performed simulation consists of the previously explained EDC test with a simulation time of 500 s. Fig. 8 shows the wind speed and the wind direction with respect to the initial tower reference frame, as described before. In the upper plot, the wind speed is decomposed into two perpendicular components in the tower frame: v_x in the fore–aft direction x_0, and v_y in the side–side direction y_0. As shown in the lower plot of Fig. 8, the wind speed is initially frontal to the nacelle; then, at 200 s, the wind direction suddenly changes to −30°. The described yaw controller reacts and rotates the nacelle until reducing misalignment with the new mean wind direction, as shown in Fig. 3. The nacelle yaw angle θ with respect to the initial tower reference frame is also shown in Fig. 8. To be used by the TFC and AGTC, the fore–aft and side–side velocities in the tower frame are

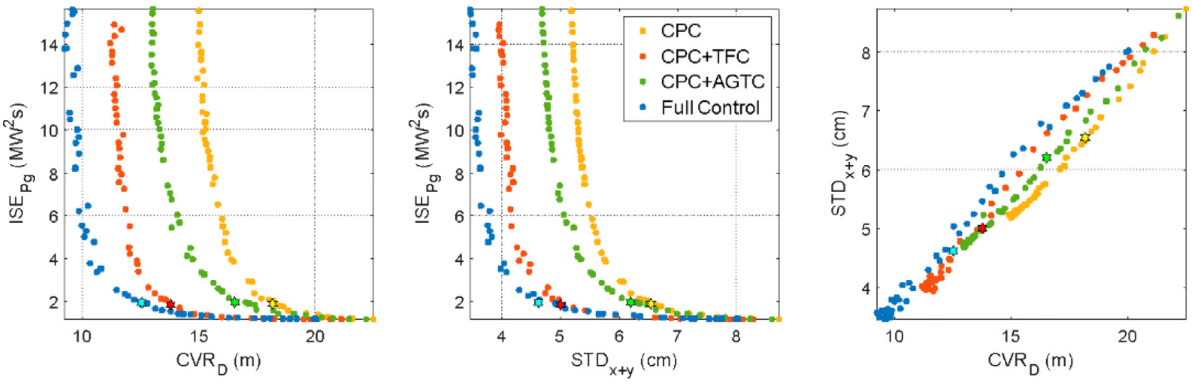

Fig. 6. 2D projections of the Pareto fronts.

Table 2
Optimal controller parameters and objective indices.

Control system	K_P (°/rpm)	T_I (s)	K_{FA} (° s/m)	K_{SS} (N s)	ISE_{Pg} (MW^2 s)	CVR_D (m)	STD_{x+y} (cm)
Full control	0.0656	24.0652	11.7448	17253	1.9528	**12.520**	**4.63**
CPC+TFC	0.0617	19.5722	9.4916	–	**1.8444**	13.773	5.01
CPC+AGTC	0.0550	11.6085	–	14738	1.9603	16.549	6.19
CPC	0.0547	13.1614	–	–	1.8824	18.167	6.54

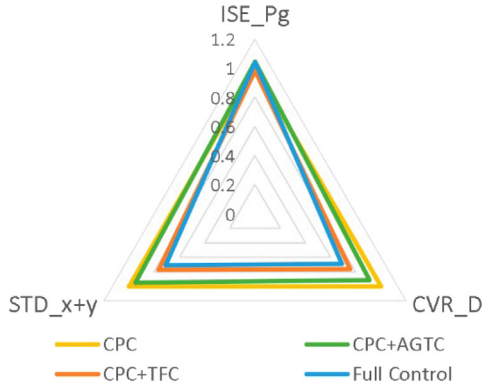

Fig. 7. Normalized spider diagram in the CPC solution for optimized objectives.

transformed into the nacelle frame by means of the rotation matrix in (8).

Fig. 9 shows the time responses obtained for each control system. Specifically, the plotted variables are the generated power, the turbine angular speed in the high side shaft, the pitch signal, and the generator torque. Tower displacements are shown in Fig. 10, both in the initial tower reference frame and in the nacelle reference frame. Figs. 9 and 10 also show a zoom of the signals from 180 to 200 s, before the EDC event, to better appreciate the differences in the time responses. Furthermore, the CVR and standard deviation of different signals are calculated as performance indices for comparison and collected in Tables 3 and 4, respectively. These tables show in parentheses the percentage of improvement or worsening of each index with respect to the CPC.

No important differences are observed in the power output and the angular speed between the different control systems, as was expected from the similar values of ISE_{Pg} in Table 2. Although the CVRs of P_g for Full Control and AGTC are higher than those obtained for CPC and CPC+TFC, as listed in Table 3, the STDs of P_g and ω_g are almost the same for all control systems, as shown in Table 4.

Before the EDC event, both the nacelle angle and the wind direction are along the x_0-axis, and the tower reference frame and the nacelle frame match. As shown in Fig. 10, the fore–aft displacements $x_{FA,0}$ (and $x_{FA,\theta}$) oscillate around 0.25 m. The side–side displacements $y_{SS,0}$ (and $y_{SS,\theta}$) vibrate around only −0.05 m because the wind component in this direction, the y_0-axis, is almost zero. These static displacements $y_{SS,0}$ are mainly due to the aerodynamic torque at the rotor. However, after the wind EDC event, the nacelle reference frame is rotated. In the two upper graphs of Fig. 10, the new rotated state produces a change in the tower static displacements in the tower reference frame. The new $x_{FA,0}$ displacements oscillate around 0.2 m; the new $y_{SS,0}$ side–side displacements are around −0.17 m because there is a greater component of the tower oscillation in the y_0-axis due to the new wind orientation. Alternatively, the two bottom plots of Fig. 10 show the fore–aft and side–side tower vibrations in the moving nacelle reference frame, where $x_{FA,\theta}$ and $y_{SS,\theta}$ oscillate around 0.25 m and −0.05 m, respectively, throughout the entire simulation. These graphs allow us to better check the damping performed by each controller in each component (fore–aft or side–side) because the static displacements are independent of the nacelle yaw angle.

The fore–aft oscillations $x_{FA,\theta}$ are better compensated by the Full Control and the CPC+TFC. In comparison to the CPC, the Full Control achieves a reduction of 34.8% in the CVR of $x_{FA,\theta}$ ($CVRx_{FA,\theta}$) and 25.3% in its standard deviation ($STDx_{FA,\theta}$). The CPC+TFC shows a reduction of 36.3% in $CVRx_{FA,\theta}$ and 23.8% in $STDx_{FA,\theta}$, which are very similar to those of the Full Control. The Full Control and the CPC+TFC obtain similar results, which demonstrate the improvement provided by the TFC in reducing fore–aft vibrations. The CPC+AGTC does not provide improvement in these indices. These values are collected in Tables 3 and 4. On the other hand, the side–side vibrations $y_{SS,\theta}$ are considerably reduced by the Full Control and the CPC+AGTC, as was expected. The Full Control reduces the CVR of these vibrations ($CVRy_{SS,\theta}$) by 62.8% and the $STDy_{SS,\theta}$ by 47.9%. The percentage reductions achieved by the CPC+AGTC in these indices are 53.7% and 41.5%, respectively, which are slightly lower than those of the Full Control. However, these values evidence the positive effect of AGTC on mitigating side–side oscillations. The CPC+TFC only provides half the damping on these vibrations, with percent reductions of 30.3% in $CVRy_{SS,\theta}$ and 23.5% in $STDy_{SS,\theta}$.

Fig. 11 shows the horizontal plane positions of the tower top in both reference frames: the tower frame and the nacelle frame. By observing simultaneously both vibration components of the tower top in this figure, the total tower displacements are analyzed. On the left side with the tower displacements in the tower reference frame, there are two fuzzy regions corresponding to the states before and after the EDC event. The left region corresponds to the first state, where the wind direction matches the x_0-axis. The right region corresponds to the second state, where the wind arrives with an orientation of −30° and the tower oscillations arise mainly in that direction. Both fuzzy regions associated with the Full Control are smaller than those associated with the other control systems, implying lower tower oscillations. On the right side, with the displacements in the nacelle reference frame, there is only a fuzzy region because this frame is independent of the yaw angle. Similarly, the Full Control shows the smallest region, which also proves the better damping of tower oscillations. This statement is also supported by a higher reduction in the peak of the frequency response of the displacements $x_{FA,\theta}$ and $y_{SS,\theta}$, as shown in Fig. 12, which displays the Fast Fourier Transformation (FFT) of the tower displacements in the nacelle reference frame. The Full Control achieves the greatest reduction, about 84%, in both peaks of $x_{FA,\theta}$ and $y_{SS,\theta}$ around the frequency of 0.33 Hz compared with the CPC, which shows the highest peak values. The CPC+TFC only reduces the peak of fore–aft displacements, whereas the CPC+AGTC only affects the peak of side–side oscillations.

However, these improvements in vibration mitigation are achieved at the expense of larger values of the generated torque and pitch signal, as shown in Fig. 9. To reduce the fore–aft vibrations, the Full Control and the CPC+TFC produce pitch signals with higher CVR values (CVR_β), which are collected in Table 3. To reduce the side–side displacements, the Full Control and the AGTC+CPC need to generate oscillations in the torque signal in comparison to CPC+TFC and CPC, where the torque remains fixed

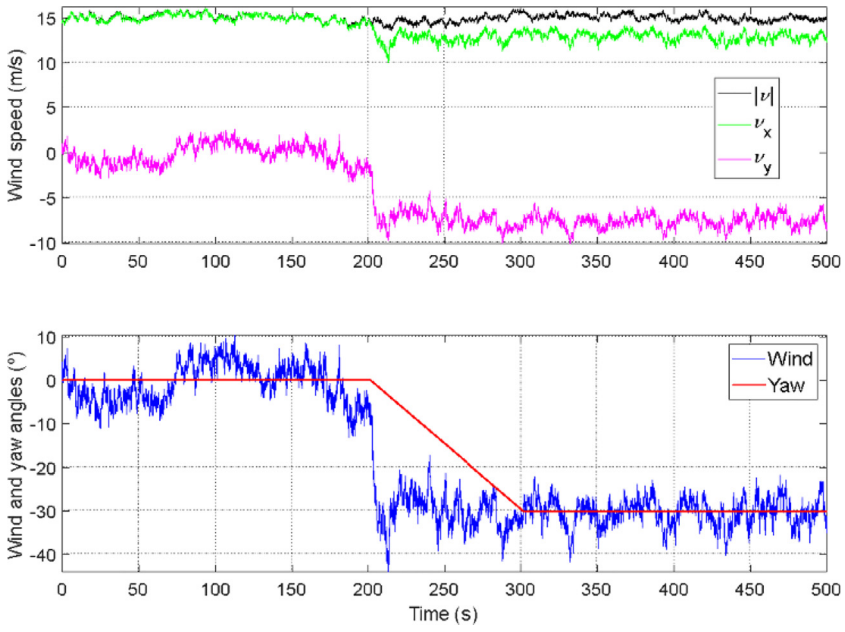

Fig. 8. Wind speed, wind angle, and nacelle yaw angle in the EDC simulation test.

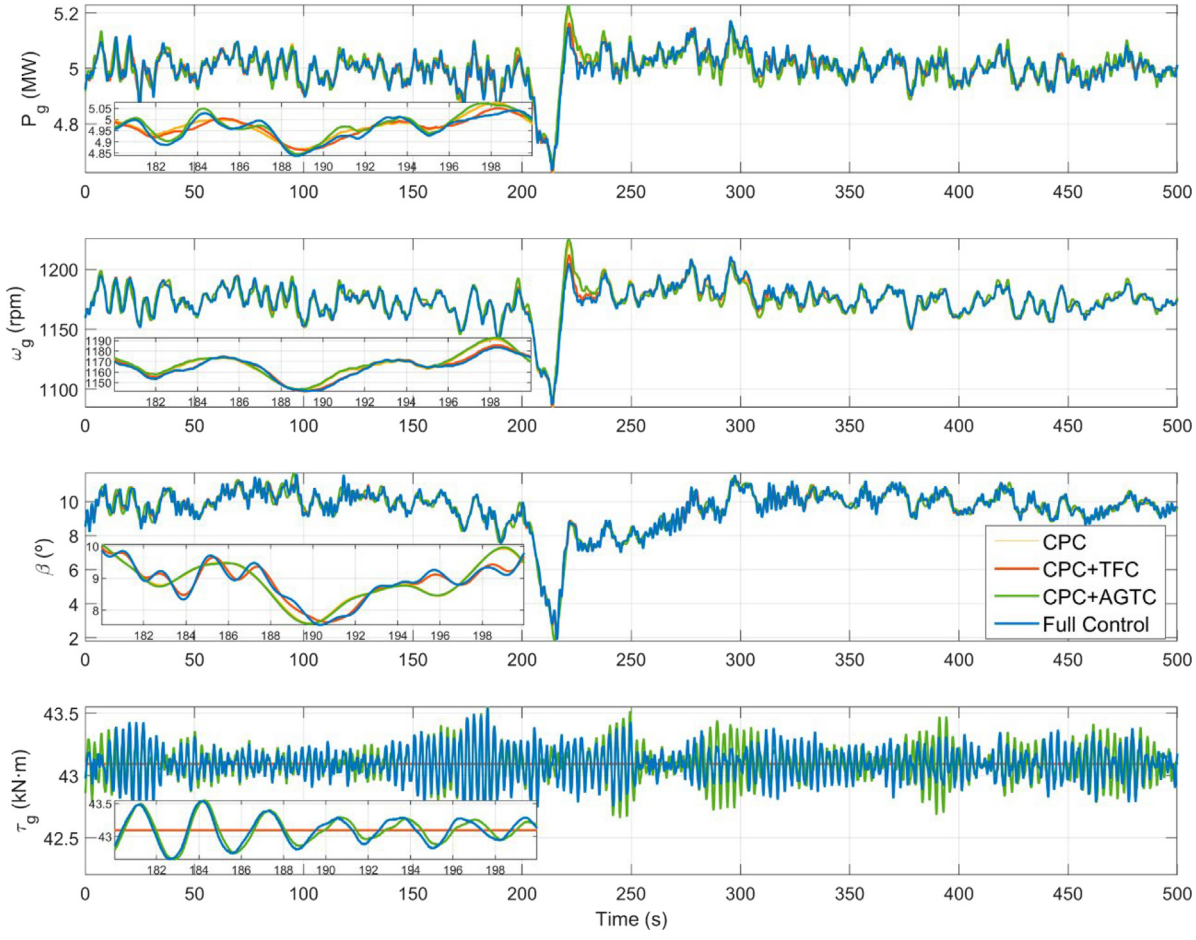

Fig. 9. Time responses of the generated power, turbine speed, pitch, and generator torque.

at its rated value. The Full Control gains the benefits of both ATDC (TFC and AGTC) without incurring high pitch control signals compared to those of the CPC+TFC or higher generator torque values than those of the CPC+AGTC.

Fig. 13 shows a spider diagram for the seven performance indices from Tables 3 and 4: $CVRx_{FA,\theta}$, $CVRy_{SS,\theta}$, the CVRs of the fore–aft and side–side moments in the nacelle reference frame ($CVRM_{FA,\theta}$ and $CVRM_{SS,\theta}$, respectively), STD_{Pg}, $STDx_{FA,\theta}$, and

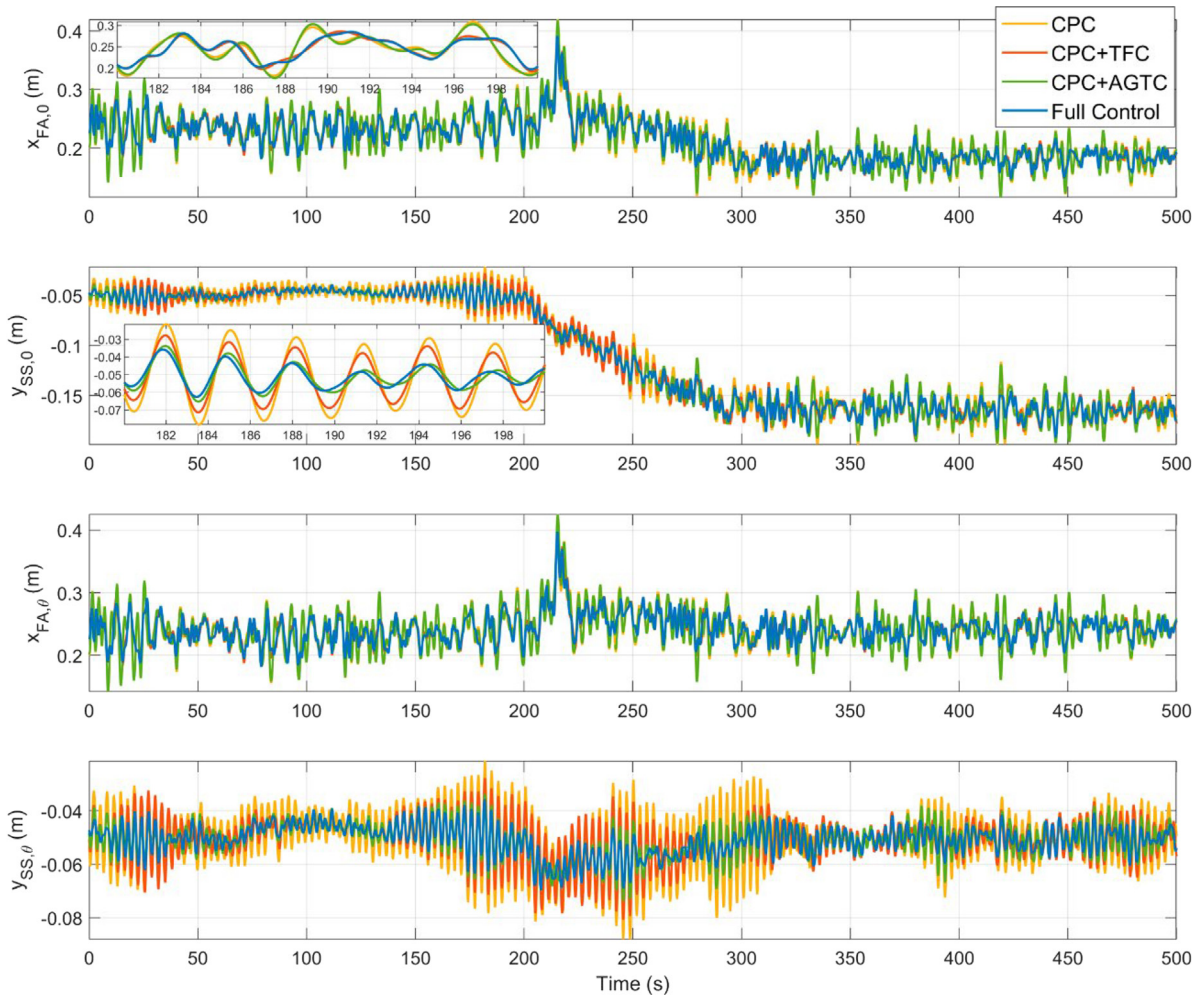

Fig. 10. Time responses of the fore–aft and side–side displacements both in the tower reference frame and in the nacelle reference frame.

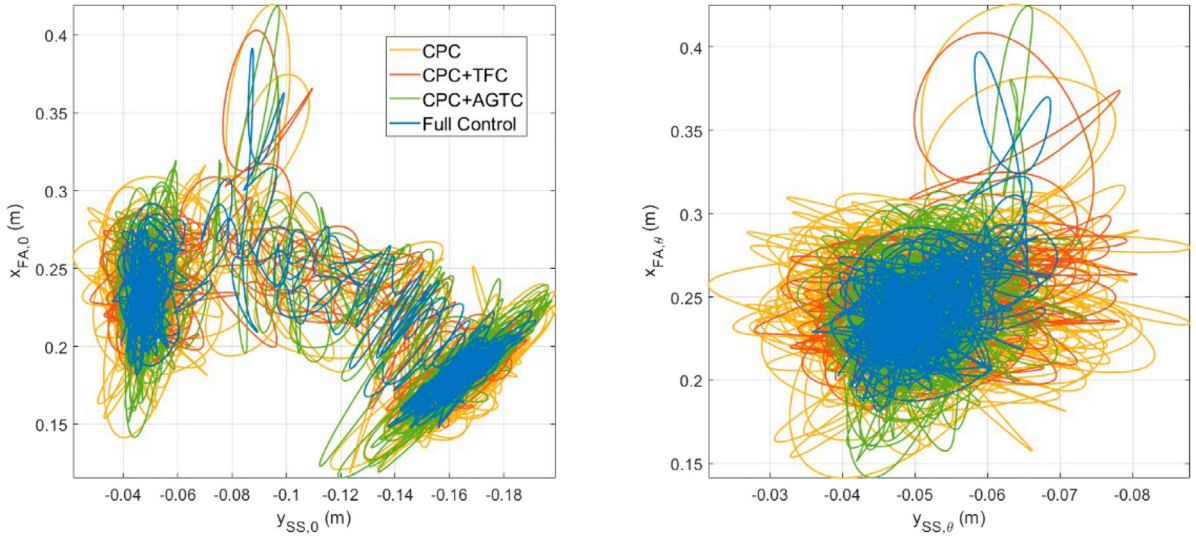

Fig. 11. Tower displacements both in the tower reference frame and in the nacelle reference frame.

$STDy_{SS,\theta}$. These indices are standardized with respect to the values of the CPC. All control systems show practically the same standard deviation of the generated power, STD_{Pg}. This index is related to the ISE_{Pg}, which was used as a cost index in the performed optimization for tuning the controllers, with similar resulting values, as shown in Table 2. Nevertheless, the diagram of Fig. 13 shows a substantial improvement in the indices associated with the fore–aft tower oscillations ($CVRx_{FA,\theta}$ and $STDx_{FA,\theta}$) for the control systems with TFC: the Full Control and the CPC+TFC. These indices are related to the optimized objectives CVR_D and

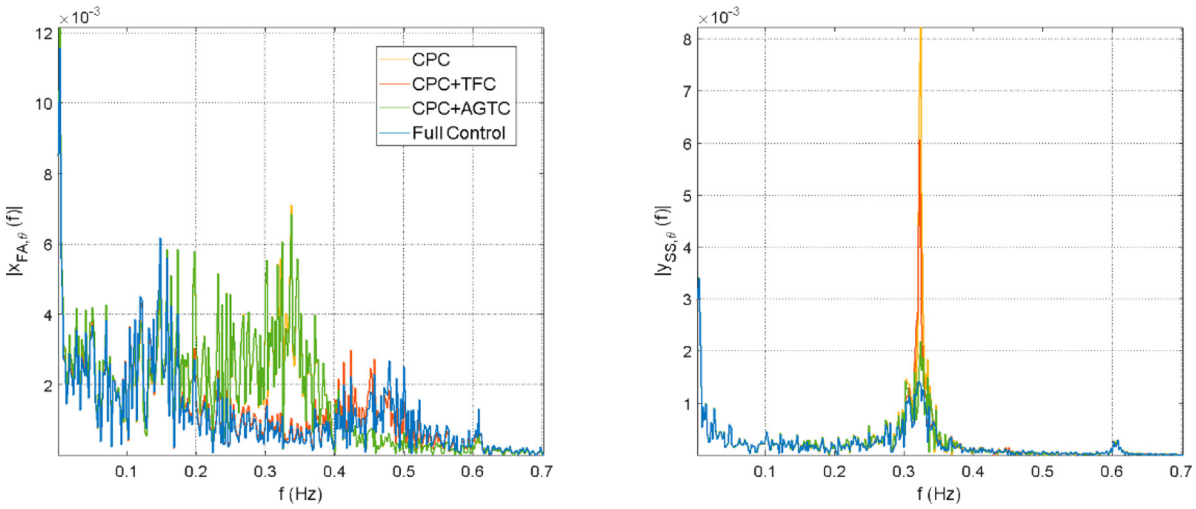

Fig. 12. Fourier amplitude of displacements $x_{FA,\theta}$ and $y_{SS,\theta}$.

Table 3
CVR of different variables and their relative change with respect to the CPC values.

Control system	CVR$x_{FA,\theta}$ (m)	CVR$y_{SS,\theta}$ (m)	CVRM$_{FA,\theta}$ (kN m 10^6)	CVRM$_{SS,\theta}$ (kN m 10^6)	CVR$_\beta$ (°)	CVR$_{Tg}$ (kN m)	CVR$_{Pg}$ (MW)	CVRω_g (rpm)
Full control	11.65 (−34.8%)	**2.96 (−62.8%)**	**2.527 (−23.3%)**	**1.569 (−27.4%)**	304.2 (+126.4%)	146.9	22.3 (+82.4%)	2976 (+7.7%)
CPC+TFC	**11.39 (−36.3%)**	5.54 (−30.3%)	2.555 (−22.5%)	1.75 (−19%)	240 (+78.6%)	0	12.64 (+3.5)	2870 (+3.9%)
CPC+AGTC	17.77 (−0.53%)	3.68 (−53.7%)	3.1511 (−4.38%)	1.846 (−14.6%)	136.8 (+1.82%)	142.2	21.8 (+78.9%)	2785 (+0.8%)
CPC	17.86	7.96	3.295	2.161	**134.4**	0	**12.21**	**2763**

Table 4
STD of different variables and their relative change with respect to the CPC values.

Control system	STD$x_{FA,\theta}$ (m)	STD$y_{SS,\theta}$ (m)	STD$_{Tg}$ (kN m)	STD$_{Pg}$ (kW)	STDω_g (rpm)	STD$_\beta$ (°)
Full control	**0.023 (−25.3%)**	**0.0055 (−47.9%)**	0.13	62.5 (+2.14%)	14.13 (−1.6%)	**1.23 (−1.2%)**
CPC+TFC	0.024 (−23.8%)	0.008 (−23.5%)	0	**60.7 (−0.73%)**	14.26 (−0.73%)	1.232 (−1.15%)
CPC+AGTC	0.0313 (0.7%)	0.006 (−41.5%)	0.14	62.8 (+2.7%)	**14.1 (−1.87%)**	1.26 (+1.04%)
CPC	0.031	0.0106	0	61.2	14.36	1.25

STD$_{x+y}$. Additionally, these control systems present a reduction of about 23% in the CVRM$_{FA,\theta}$. In the same way, the control systems with AGTC (the Full Control and the CPC+AGTC) obtain the smallest values of the indices related to the side–side tower vibrations. They achieve reductions greater than 50% in the CVR$y_{SS,\theta}$ and 40% in the STD$y_{SS,\theta}$. The Full Control achieves the largest reduction of 27.4% of the CVRM$_{SS,\theta}$, whereas the CPC+TFC slightly outperforms the CPC+AGTC on this index. These results indicate that the Full Control achieves a good balance between different performance indices.

Finally, although this work focuses only on the tower loads, the five main fatigue loads of a wind turbine, which are depicted in Fig. 1, are compared in Table 5, where the damage equivalent load (DEL) is used as a measure of fatigue load. The table includes the DEL of the tower base fore–aft moment DEL$_{FA}$, the DEL of the tower base side–side moment DEL$_{SS}$, the DEL of the low-speed shaft torsion moment DEL$_{LSST}$, the DEL of the blade flap-wise moment DEL$_{FW}$, and the DEL of the blade edgewise moment DEL$_{EW}$. As expected, the proposed Full Control achieves the smallest DEL values related to the tower moments. The DEL related to the blade edgewise moment is the same for all control systems. The DEL of the blade flap-wise moment and the DEL of the low-speed shaft torsion moment are increased about 8% and 10%, respectively, by the Full Control and the CPC+TFC; therefore, this increment must have been produced by the TFC action. Note that no wind turbine variables closely related to the last three DELs have been considered in the optimization procedure.

5. Conclusions

A wind turbine control structure that operates on the pitch and torque variables in the full load zone has been developed for a 5 MW wind turbine. The proposed control strategy mainly combines three control loops: a PI controller, which regulates the turbine speed by actuating on the pitch angle, a proportional tower-feedback control, which generates an extra pitch signal to reduce fore–aft displacements, and a proportional active generator-torque control, which mitigates the tower side–side oscillations. A multi-objective optimization based on genetic algorithms has been proposed to obtain Pareto front solutions for a problem that considers three objective functions: one related to the generated power error (ISE of generated power), and the other two related to tower vibrations. These last two are the CVR of the total displacements, which is related to the frequency,

Table 5
DEL of different fatigue loads and their relative change with respect to the CPC values.

Control system	DEL_{FA} (kN m)	DEL_{SS} (kN m)	DEL_{LSST} (kN m)	DEL_{FW} (kN m)	DEL_{EW} (kN m)
Full control	**$8.74 \cdot 10^3$ (−28.18%)**	**$4.79 \cdot 10^3$ (−19.09%)**	193.73 (+10.39%)	$3.35 \cdot 10^3$ (+7.71%)	$6.072 \cdot 10^3$ (+0.03%)
CPC+TFC	$9.18 \cdot 10^3$ (−24.57%)	$5.24 \cdot 10^3$ (−11.49%)	190.55 (+8.58%)	$3.37 \cdot 10^3$ (+8.36%)	$6.072 \cdot 10^3$ (+0.03%)
CPC+AGTC	$12.12 \cdot 10^3$ (−0.41%)	$5.37 \cdot 10^3$ (−9.29%)	172.5 (−1.71%)	$3.21 \cdot 10^3$ (+3.22%)	$6.069 \cdot 10^3$ (−0.02%)
CPC	$12.17 \cdot 10^3$	$5.92 \cdot 10^3$	**175.5**	**$3.11 \cdot 10^3$**	$6.07 \cdot 10^3$

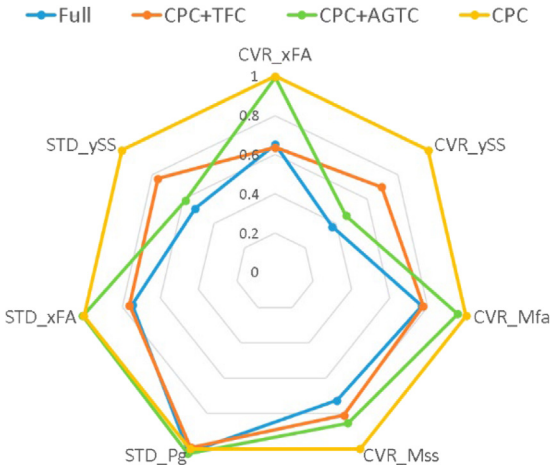

Fig. 13. Spider diagram for different performance indices.

and the sum of standard deviations of fore–aft and side–side displacements, which is related to the oscillation amplitude. The optimization procedure was performed by simulation through MATLAB/Simulink with the assistance of FAST for the nonlinear wind turbine model. The simulation used in the optimization procedure was based on the wind Extreme Direction Change event defined in the IEC 61400–1 standard. The Pareto solutions were analyzed with multiple MCDM methods, and an average solution was chosen as the optimal one. Other simpler control schemes were also calculated and simulated similarly for comparison: a PI controller without any active damping control, a PI controller with TFC, and a PI controller with AGTC.

The quantitative analysis of the simulation results confirms that the proposed approach based on multi-objective optimization yields a good compromise between the generated wind power and tower vibration damping. In comparison to the CPC, the proposed Full Control achieves reductions of about 35% and 25% in the CVR and STD of fore–aft displacements, respectively, and about 63% and 48% in the CVR and STD of side–side oscillations, respectively. This superior performance in terms of tower vibration reduction is achieved at the expense of increasing the DELs of flap-wise moment and low shaft speed torsion moment, as well as the CVR of the control signals of the pitch and the generator torque. The maintenance costs of the pitch mechanism could be uneconomically high, potentially negating any benefit in reducing moments on the structure. The optimized indices STD_{x+y} and CVR_D of the tower vibrations are correlated and therefore, reducing one of them implies reducing the other. Consequently, in further works, one of these indices can be substituted by other objectives to be investigated, such as the CVR of the pitch actuator or indices related to the tower moments. As further research, controllers will also be developed in more detail, such as including filters to investigate the possible improvement that they provide. Additionally, the incorporation in the control system of both IPC and feedforward control with wind speed estimator will be studied, and new objectives related to blade loading mitigation will be included in the MOO and analyzed.

The proposed optimization procedure must be performed offline, which is a drawback from a viewpoint of real-time implementation. In addition, the optimal parameter tuning will vary according to the mean wind speed. Although this work only presents the optimal design for a mean wind speed, the proposed control strategy can be easily extended to adapt to changes in the mean wind speed. Further offline optimizations would need to be performed and then, the resulting optimal parameter sets would be used in a gain-scheduling control scheme having an easy real-time implementation.

Declaration of competing interest

The authors declare the following financial interests/personal relationships which may be considered as potential competing interests: Juan Garrido Jurado reports financial support and equipment, drugs, or supplies were provided by Spanish Ministry of Science and Innovation. Juan Garrido Jurado reports financial support, article publishing charges, equipment, drugs, or supplies, and travel were provided by Regional Ministry of Economic Transformation, Industry, Knowledge, and Universities of Andalusia, Spain. Manuel Lara Ortiz reports financial support was provided by Spanish Ministry of Education, Culture, and Sports.

Data availability

Data will be made available on request.

Acknowledgments

This work was supported by the Spanish Ministry of Science and Innovation (MCIN/AEI/10.13039/501100011033) under Grant PID2020-117063RB-I00 and jointly financed by the Operational Program of the European Regional Development Fund 2014–2020 and the Regional Ministry of Economic Transformation, Industry, Knowledge, and Universities of Andalusia, Spain, under Grant P18-TP-2040. M. Lara also expresses appreciation for the FPU fellowship (FPU17/02747) from the Spanish Ministry of Education, Culture, and Sports.

References

Bianchi, F., de Battista, H., Mantz, R., 2007. Wind Turbines Control Systems: Principles, Modelling and Gain Scheduling Design. Springer-Verlag, London.
Bossanyi, E.A., 2003a. Individual blade pitch control for load reduction. Wind Energy 6 (2), 119–128. http://dx.doi.org/10.1002/we.76.
Bossanyi, E.A., 2003b. Wind turbine control for load reduction. Wind Energy 6 (3), 229–244. http://dx.doi.org/10.1002/we.95.
Chiandussi, G., Codegone, M., Ferrero, S., Varesio, F.E., 2012. Comparison of multiobjective optimization methodologies for engineering applications. Comput. Math. Appl. 63 (5), 912–942. http://dx.doi.org/10.1016/j.camwa.2011.11.057.
Chitsaz, N., Banihabib, M.E., 2015. Comparison of different multi criteria decision-making models in prioritizing flood management alternatives. Water Resour. Manag. 29 (8), 2503–2525. http://dx.doi.org/10.1007/s11269-015-0954-6.

Cui, Y., Geng, Z., Zhu, Q., Han, Y., 2017. Review: Multi-objective optimization methods and application in energy saving. Energy 125, 681–704. http://dx.doi.org/10.1016/j.energy.2017.02.174.

Deb, K., Pratap, A., Agarwal, S., Meyarivan, T., 2002. A fast and elitist multiobjective genetic algorithm: NSGA-II. IEEE Trans. Evol. Comput. 6 (2), 182–197. http://dx.doi.org/10.1109/4235.996017.

Faraji Nayeh, R., Moradi, H., Vossoughi, G., 2020. Multivariable robust control of a horizontal wind turbine under various operating modes and uncertainties: A comparison on sliding mode and hinf control. Int. J. Electr. Power Energy Syst. 115, 105474. http://dx.doi.org/10.1016/j.ijepes.2019.105474.

Fischer, T., Vries, W., Rainey, P., Schmidt, B., Argyriadis, K., Kühn, M., 2012. Offshore support structure optimization by means of integrated design and controls. Wind Energy 15 (1), 99–117. http://dx.doi.org/10.1002/we.521.

Fitzgerald, B., Basu, B., Nielsen, S.R.K., 2013. Active tuned mass dampers for control of in-plane vibrations of wind turbine blades. Struct. Control Health Monit. 20 (12), 1377–1396. http://dx.doi.org/10.1002/stc.1524.

Fragoso, S., Garrido, J., Vázquez, F., Morilla, F., 2017. Comparative analysis of decoupling control methodologies and H<inf> ∞</inf>multivariable robust control for variable-speed, variable-pitch wind turbines: Application to a lab-scale wind turbine. Sustainability (Switzerland) 9 (5), http://dx.doi.org/10.3390/su9050713.

Galán-Lavado, A., Santos, M., 2021. Analysis of the effects of the location of passive control devices on the platform of a floating wind turbine. Energies 14 (10), 2850. http://dx.doi.org/10.3390/en14102850.

Gambier, A., 2021. Pitch control of three bladed large wind energy converters—a review. Energies 14 (23), 1–24. http://dx.doi.org/10.3390/en14238083.

Gambier, A., 2022a. Control of Large Wind Energy Systems: Theory and Methods for the User. Springer.

Gambier, A., 2022b. Multiobjective optimal control of wind turbines: A survey on methods and recommendations for the implementation. Energies 15 (2), 567. http://dx.doi.org/10.3390/en15020567.

Gambier, A., Behera, A., 2018. Integrated pitch control system design of a wind turbine by using multiobjective optimization. IFAC-PapersOnLine 51 (28), 239–244. http://dx.doi.org/10.1016/j.ifacol.2018.11.708.

Gambier, A., Nazaruddin, Y.Y., 2018. Collective pitch control with active tower damping of a wind turbine by using a nonlinear PID approach. IFAC-PapersOnLine 51 (4), 238–243. http://dx.doi.org/10.1016/j.ifacol.2018.06.072.

Garcia-Sanz, M., Houpis, C.H., 2012. Wind Energy Systems. CRC Press, http://dx.doi.org/10.1201/b11673.

Golnary, F., Tse, K.T., 2022. Simultaneous active control of tower lateral vibration and power control of wind turbine: A novel multivariable approach. Energy Rep. 8, 4233–4251. http://dx.doi.org/10.1016/j.egyr.2022.03.083.

He, E.-M., Hu, Y.-Q., Zhang, Y., 2017. Optimization design of tuned mass damper for vibration suppression of a barge-type offshore floating wind turbine. Proc. Inst. Mech. Eng. M 231 (1), 302–315. http://dx.doi.org/10.1177/1475090216642466.

IEC 61400–1, 2005. Wind Turbines - Part 1: Design Requirements.

Jonkman, B.J., 2009. Turbsim User's Guide: Version 1.50. http://dx.doi.org/10.2172/965520.

Jonkman, J.M., Buhl, Jr., M.L., 2005. FAST User's Guide. NREL/EL-500-29798.

Jonkman, J.M., Butterfield, S., Musial, W., Scott, G., 2009. Definition of a 5-MW Reference Wind Turbine for Offshore System Development.

Kong, X., Cai, C.S., Hu, J., 2017. The state-of-the-art on framework of vibration-based structural damage identification for decision making. Appl. Sci. (Switzerland) 7 (5), http://dx.doi.org/10.3390/app7050497.

Lackner, M.A., Rotea, M.A., 2011. Passive structural control of offshore wind turbines. Wind Energy 14 (3), 373–388. http://dx.doi.org/10.1002/we.426.

Lara, M., Garrido, J., Ruz, M.L., Vázquez, F., 2021. Adaptive pitch controller of a large-scale wind turbine using multi-objective optimization. Appl. Sci. (Switzerland) 11 (6), http://dx.doi.org/10.3390/app11062844.

Lee, H.-C., Chang, C.-T., 2018. Comparative analysis of MCDM methods for ranking renewable energy sources in Taiwan. Renew. Sustain. Energy Rev. 92, 883–896. http://dx.doi.org/10.1016/j.rser.2018.05.007.

Lee, J., Zhao, F., 2022. GWEC Global Wind Report. Global Wind Energy Council, p. 75.

Lin, Z., Chen, Z., Liu, J., Wu, Q., 2019. Coordinated mechanical loads and power optimization of wind energy conversion systems with variable-weight model predictive control strategy. Appl. Energy 236, 307–317. http://dx.doi.org/10.1016/j.apenergy.2018.11.089.

Lin, Z., Chen, Z., Wu, Q., Yang, S., Meng, H., 2018. Coordinated pitch & torque control of large-scale wind turbine based on Pareto efficiency analysis. Energy 147, 812–825. http://dx.doi.org/10.1016/j.energy.2018.01.055.

Liu, H., Tang, Q., Chi, Y., Zhang, Z., Yuan, X., 2016. Vibration reduction strategy for wind turbine based on individual pitch control and torque damping control. Int. Trans. Electr. Energy Syst. 26 (10), 2230–2243. http://dx.doi.org/10.1002/etep.2201.

Luo, L., Zhang, X., Song, D., Tang, W., Li, L., Tian, X., 2019. Minimizing the energy cost of offshorewind farms by simultaneously optimizing wind turbines and their layout. Appl. Sci. (Switzerland) 9 (5), http://dx.doi.org/10.3390/app9050835.

Mahdizadeh, A., Schmid, R., Oetomo, D., 2021. LIDAR-assisted exact output regulation for load mitigation in wind turbines. IEEE Trans. Control Syst. Technol. 29 (3), 1102–1116. http://dx.doi.org/10.1109/TCST.2020.2991640.

Mensah, A.F., Dueñas-Osorio, L., 2014. Improved reliability of wind turbine towers with tuned liquid column dampers (TLCDs). Struct. Saf. 47, 78–86. http://dx.doi.org/10.1016/j.strusafe.2013.08.004.

Novaes Menezes, E.J., Araújo, A.M., Bouchonneau da Silva, N.S., 2018. A review on wind turbine control and its associated methods. J. Clean. Prod. 174, 945–953. http://dx.doi.org/10.1016/j.jclepro.2017.10.297.

Odgaard, P.F., Larsen, L.F.S., Wisniewski, R., Hovgaard, T.G., 2016. On using Pareto optimality to tune a linear model predictive controller for wind turbines. Renew. Energy 87, 884–891. http://dx.doi.org/10.1016/j.renene.2015.09.067.

Park, S., Glade, M., Lackner, M.A., 2020. Multi-objective optimization of orthogonal TLCDs for reducing fatigue and extreme loads of a floating offshore wind turbine. Eng. Struct. 209, 110260. http://dx.doi.org/10.1016/j.engstruct.2020.110260.

Pascu, V., Kanev, S., van Wingerden, J.-W., 2017. Adaptive tower damping control for offshore wind turbines. Wind Energy 20 (5), 765–781. http://dx.doi.org/10.1002/we.2058.

Poureh, A., Nobakhti, A., 2020. Mode decomposition approach in robust control design for horizontal axis wind turbines. Wind Energy 23 (2), 312–326. http://dx.doi.org/10.1002/we.2431.

Ruz, M.L., Garrido, J., Fragoso, S., Vazquez, F., 2020. Improvement of small wind turbine control in the transition region. Processes 8 (2), http://dx.doi.org/10.3390/pr8020244.

Saravanakumar, R., Jena, D., 2015. Validation of an integral sliding mode control for optimal control of a three blade variable speed variable pitch wind turbine. Int. J. Electr. Power Energy Syst. 69, 421–429. http://dx.doi.org/10.1016/j.ijepes.2015.01.031.

Schlipf, D., Schlipf, D.J., Kühn, M., 2013. Nonlinear model predictive control of wind turbines using LIDAR. Wind Energy 16 (7), 1107–1129. http://dx.doi.org/10.1002/we.1533.

Sierra-García, J.E., Santos, M., 2020. Performance analysis of a wind turbine pitch neurocontroller with unsupervised learning. Complexity 2020, 1–15. http://dx.doi.org/10.1155/2020/4681767.

Sierra-García, J.E., Santos, M., 2021. Redes neuronales y aprendizaje por refuerzo en el control de turbinas eólicas. Rev. Iberoam. Autom. Inform. Ind. 18 (4), 327. http://dx.doi.org/10.4995/riai.2021.16111.

Sierra-Garcia, J.E., Santos, M., 2022. Deep learning and fuzzy logic to implement a hybrid wind turbine pitch control. Neural Comput. Appl. 34 (13), 10503–10517. http://dx.doi.org/10.1007/s00521-021-06323-w.

Sierra-Garcia, J.E., Santos, M., Pandit, R., 2022. Wind turbine pitch reinforcement learning control improved by PID regulator and learning observer. Eng. Appl. Artif. Intell. 111, 104769. http://dx.doi.org/10.1016/j.engappai.2022.104769.

Song, D., Tu, Y., Wang, L., Jin, F., Li, Z., Huang, C., Xia, E., Rizk-Allah, R.M., Yang, J., Su, M., Hoon Joo, Y., 2022. Coordinated optimization on energy capture and torque fluctuation of wind turbines via variable weight NMPC with fuzzy regulator. Appl. Energy 312, http://dx.doi.org/10.1016/j.apenergy.2022.118821.

Spencer, M., Stol, K., Cater, J., 2012. Predictive yaw control of a 5MW wind turbine model. In: 50th AIAA Aerospace Sciences Meeting Including the New Horizons Forum and Aerospace Exposition. http://dx.doi.org/10.2514/6.2012-1020.

Sun, C., 2018. Semi-active control of monopile offshore wind turbines under multi-hazards. Mech. Syst. Signal Process. 99, 285–305. http://dx.doi.org/10.1016/j.ymssp.2017.06.016.

Villoslada, D., Santos, M., Tomás-Rodríguez, M., 2021. General methodology for the identification of reduced dynamic models of barge-type floating wind turbines. Energies 14 (13), 3902. http://dx.doi.org/10.3390/en14133902.

Villoslada, D., Santos, M., Tomás-Rodríguez, M., 2022. TMD stroke limiting influence on barge-type floating wind turbines. Ocean Eng. 248, 110781. http://dx.doi.org/10.1016/j.oceaneng.2022.110781.

Viveiros, C., Melício, R., Igreja, J.M., Mendes, V.M.F., 2015. Supervisory control of a variable speed wind turbine with doubly fed induction generator. Energy Rep. 1, 89–95. http://dx.doi.org/10.1016/j.egyr.2015.03.001.

Wakui, T., Nagamura, A., Yokoyama, R., 2021. Stabilization of power output and platform motion of a floating offshore wind turbine-generator system using model predictive control based on previewed disturbances. Renew. Energy 173, 105–127. http://dx.doi.org/10.1016/j.renene.2021.03.112.

Wang, N., Johnson, K.E., Wright, A.D., 2013. Comparison of strategies for enhancing energy capture and reducing loads using LIDAR and feedforward control. IEEE Trans. Control Syst. Technol. 21 (4), 1129–1142. http://dx.doi.org/10.1109/TCST.2013.2258670.

Wang, P., Zhu, Z., Wang, Y., 2016. A novel hybrid MCDM model combining the SAW, TOPSIS and GRA methods based on experimental design. Inform. Sci. 345, 27–45. http://dx.doi.org/10.1016/j.ins.2016.01.076.

Yin, M., Li, W., Chung, C.Y., Zhou, L., Chen, Z., Zou, Y., 2017. Optimal torque control based on effective tracking range for maximum power point tracking of wind turbines under varying wind conditions. IET Renew. Power Gener. 11 (4), 501–510. http://dx.doi.org/10.1049/iet-rpg.2016.0635.

Yin, M., Yang, Z., Xu, Y., Liu, J., Zhou, L., Zou, Y., 2018. Aerodynamic optimization for variable-speed wind turbines based on wind energy capture efficiency. Appl. Energy 221, 508–521. http://dx.doi.org/10.1016/j.apenergy.2018.03.078.

Yuan, Y., Tang, J., 2017. Adaptive pitch control of wind turbine for load mitigation under structural uncertainties. Renew. Energy 105, 483–494. http://dx.doi.org/10.1016/j.renene.2016.12.068.

Zhang, Z., Nielsen, S.R.K., Blaabjerg, F., Zhou, D., 2014. Dynamics and control of lateral tower vibrations in offshore wind turbines by means of active generator torque. Energies 7 (11), 7746–7772. http://dx.doi.org/10.3390/en7117746.

Zuo, H., Bi, K., Hao, H., 2020. A state-of-the-art review on the vibration mitigation of wind turbines. Renew. Sustain. Energy Rev. 121, 109710. http://dx.doi.org/10.1016/j.rser.2020.109710.